SCIENCE CHINA
Physics, Mechanics & Astronomy

•Article•

March 2022 Vol. 65 No. 3: 239511
https://doi.org/10.1007/s11433-021-1828-y

Terahertz superconducting kinetic inductance detectors demonstrating photon-noise-limited performance and intrinsic generation-recombination noise

Qing Shi[1,2], Jing Li[1], Qiang Zhi[1,2], Zheng Wang[1], Wei Miao[1], and Sheng-Cai Shi[1*]

[1] *Purple Mountain Observatory, Chinese Academy of Sciences, Nanjing 210034, China;*
[2] *School of Astronomy & Space Science, University of Science and Technology of China, Hefei 230026, China*

Received September 29, 2021; accepted December 3, 2021; published online January 11, 2022

The development of large-format detector arrays with background-limited performance is of particular interest at the terahertz (THz) band, which is a unique band in search of our cosmic origins. With high sensitivity and being more promising in the pixel number and multiplexing technology, superconducting kinetic inductance detectors (KID) are emerging as a major choice of detectors of this type. Here we fabricate three-THz-band (0.35/0.85/1.4 THz) KIDs on a single chip from a 120-nm-thick aluminum (Al) superconducting film and measure photon-noise-limited performance and intrinsic generation-recombination noise at high (>1 pW) and low (<1 fW) optical radiation power, respectively. Their responses to blackbody (optical) radiation are proven to be purely from photons compared with the responses of two dark KIDs intentionally arranged on the same detector chip. The lowest optical noise equivalent power (NEP) reaches 6×10^{-18} W/Hz$^{0.5}$ and the optical coupling efficiency is in the range of 49%-56% for the three KIDs, which are in good agreement with the simulation results.

terahertz, kinetic inductance detectors (KID), photon-noise, generation-recombination noise

PACS number(s): 85.25.pb, 07.20.Mc, 07.57.-c, 07.57.kp

Citation: Q. Shi, J. Li, Q. Zhi, Z. Wang, W. Miao, and S.-C. Shi, Terahertz superconducting kinetic inductance detectors demonstrating photon-noise-limited performance and intrinsic generation-recombination noise, Sci. China-Phys. Mech. Astron. **65**, 239511 (2022), https://doi.org/10.1007/s11433-021-1828-y

1 Introduction

The terahertz (THz) band contains nearly half of the radiant photon energy in the universe, is a band with peaked thermal radiation for dark and cold celestial objects, and has rich molecular and atomic fine-structure lines [1]. Given the uniqueness in search of our cosmic origins at the THz band, the development of large-format detector arrays with background-limited performance is of particular interest. Transition-edge sensors (TES) [2] and kinetic inductance detectors (KID) [3] are currently two major choices of this type of detector. Compared with TESs, which have been applied widely in cosmic microwave background (CMB) experiments, KIDs are more appealing in the pixel number and the multiplexing technology, but yet to demonstrate full capability on astronomical telescopes [4]. China is planning to build a THz telescope in Antarctica [5] or the Tibetan Plateau, with KIDs as a choice of its THz cameras.

It is well known that the surface impedance of a superconducting film, namely high-frequency loss due to quasiparticles and kinetic inductance due to Cooper pairs, is very sensitive to the coupled external fields such as optical radiation (photons) and thermal phonons [6,7]. KIDs are basically a microwave high-quality-factor (Q) resonator made

*Corresponding author (email: scshi@pmo.ac.cn)

from a superconducting film, thus being particularly suited for detection of radiation with energy excessing 2Δ (twice the superconductor's energy gap). In addition, thousands of KIDs can be read out simultaneously via frequency-domain multiplexing in a bandwidth of merely a few GHz, which is rather attractive to large-format detector arrays. The physical mechanism of KIDs is mainly the generation/recombination of quasiparticles and the quasiparticle-number fluctuation [8,9]. The fundamental limit of the sensitivity of KIDs is determined by the photon-induced noises, expressed as a noise equivalent power $\mathrm{NEP}_{\mathrm{photon}}$

$$\mathrm{NEP}_{\mathrm{photon}} = \sqrt{\frac{2P_{\mathrm{rad}}h\nu(1+n\eta_{\mathrm{opt}})+2\Delta P_{\mathrm{rad}}/\eta_{\mathrm{pb}}}{\eta_{\mathrm{opt}}}}, \quad (1)$$

where P_{rad} and η_{opt} are the optical radiation power and the total optical efficiency of the detector system, h is Plank's constant, ν the photon frequency, n the occupation number in single-mode [10], Δ the energy gap of the superconducting film at a bath temperature of T, and η_{pb} (~0.57) the efficiency of photon energy conversion to quasiparticle [11]. The term of $2P_{\mathrm{rad}}h\nu(1+n\eta_{\mathrm{opt}})/\eta_{\mathrm{opt}}$, also known as the background noise, is from the random arrival rate of photons and photon bunching and holds for all incoherent power detectors, while the term of $2\Delta P_{\mathrm{rad}}/\eta_{\mathrm{opt}}\eta_{\mathrm{pb}}$ designates the recombination noise of the quasiparticles from the Cooper pairs broken by energetic photons. Note that the generated noise of the quasiparticles is not included here as it is already included in the former term. For pair-breaking detectors like KIDs, there is also an intrinsic generation-recombination (G-R) noise of quasiparticles [12,13], with its noise equivalent power $\mathrm{NEP}_{\mathrm{G\text{-}R}}$ given by

$$\mathrm{NEP}_{\mathrm{G\text{-}R}} = \frac{2\Delta}{\eta_{\mathrm{pb}}\eta_{\mathrm{opt}}}\sqrt{\frac{N_{\mathrm{qp}}}{\tau_{\mathrm{qp}}}}, \quad (2)$$

where N_{qp} is the number of quasiparticles, and τ_{qp} the life time of quasiparticles. Note that the two noises by eqs. (1) and (2) are uncorrelated and their amplitudes add in quadrature.

Lens-antenna coupled KIDs based on an Al-NbTiN hybrid film structure [12,14-17] and lumped-element KIDs based on a single TiN or Al thin film [18,19] have demonstrated the photon-noise limited sensitivity in a single THz frequency band. Recently a lens-antenna coupled KID at 1.54 THz based on ultra-thin Al film exhibited the intrinsic G-R noise as well as the photon-noise limited sensitivity [9]. Given the fact that the THz background noise at Dome A in Antarctic is at the level of 10^{-16} W/Hz$^{0.5}$, we are planning to develop large format (>1 k pixels) lens-antenna coupled THz KID arrays based on a single Al film of a relatively large thickness (>100 nm), which is beneficial to the uniformity of large format arrays. This paper focuses on the study of the sensitivity limit and optical efficiency of three Al KIDs on a single chip at 0.35, 0.85 and 1.4 THz, which correspond to three atmospheric widows at Dome A in Antarctic, with the last two rarely accessible for other sites on Earth [1].

2 Experimental details

As shown in Figure 1(a), the designed experimental detector chip includes 0.35/0.85/1.4 THz KIDs, marked as detector 1, 2, and 3, which are made up of a microwave superconducting resonator and an integrated THz twin-slot antenna at the detector's readout frequency and the optical radiation band, respectively. Each KID absorbs THz photons through the integrated twin-slot antenna and an ellipsoidal silicon lens attached to the detector chip, which is a typical combination for lens-antenna coupled detectors. As it is well known,

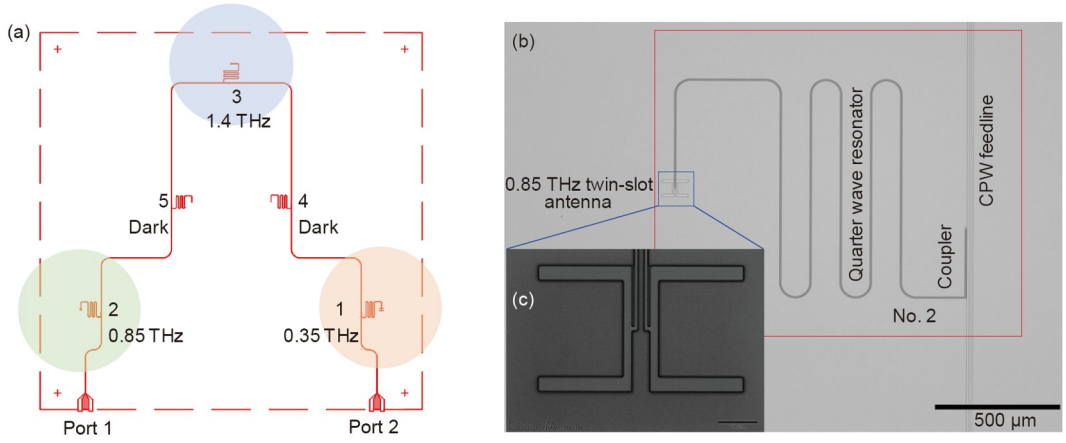

Figure 1 (Color online) (a) Layout of the designed experimental detector chip. It consists of three-THz-band KIDs (0.35/0.85/1.4 THz, marked as detector 1, 2, and 3) and two dark KIDs (marked as detector 4 and 5). The three-THz-band KIDs are made up of a microwave superconducting resonator and an integrated THz twin-slot antenna, while the two dark KIDs have no integrated THz antenna. The light red, light green and light blue areas indicate the locations of respective ellipsoidal silicon lenses for THz radiation coupling. (b) Optical microscopic image of the 0.85-THz KID, which includes a coupler, a quarter-wavelength CPW short-circuited resonator, and a 0.85-THz twin-slot antenna. (c) A detailed view of the 0.85-THz twin-slot antenna.

photons and thermal phonons have similar effects on the resonance/transmission response of KIDs [20], i.e., lowering the resonance frequency and quality factor, so long as their energy is sufficiently high to break Cooper pairs in the superconducting film (for we Al, $\Delta\approx193$ μeV). On the other hand, optical radiation may increase somewhat the local ambient temperature of the measured detector chip, thus resulting in a mixed response owing to photons and thermal phonons. To verify the measured responses of the three KIDs coming only from optical radiation, we added two dark KIDs (i.e., no optical radiation coupling) on the designed detector chip for comparison, marked as detectors 4 and 5. The five KIDs have microwave resonance frequencies distributed in the range of 4-5 GHz and their transmission responses are read out through a common 50-Ω CPW line (6-μm gap and 10-μm wide central conductor). Figure 1(b) and (c) show the 0.85-THz KID on the experimental detector chip, which is fabricated from a 120-nm thick Al film evaporated on a 350-μm thick high-resistivity silicon substrate (same as the other KIDs).

Like conventional lens-antenna coupled KIDs, the 0.85-THz KID includes a coupler, a 4.6 GHz (arbitrarily chosen in the frequency range of our measurement system) quarter-wavelength CPW (2-μm gap and 3-μm wide central conductor) short-circuited resonator, and a 0.85-THz twin-slot antenna. Note that THz radiation received by the twin-slot antenna breaks Cooper pairs in the center conductor of the antenna's CPW feedline and the excited quasiparticles diffuse within a length of $l=(D\tau_{qp})^{0.5}$ (for Al films, D=60 cm^2/s, τ_{qp} is the quasiparticle lifetime) [21].

The experimental setup consists of a temperature-variable blackbody, a set of optical filters, the measured detectors, and a room-temperature homodyne readout system, with the first three components shown in Figure 2. The temperature-variable blackbody and the optical filter set are combined to provide a three-THz-band radiation source for this experiment. As shown in Figure 2(b), an oxygen-free copper block accommodating the detector chip and three elliptical silicon lenses are installed on the mixing chamber of a dilution fridge whose temperature can vary from 60 to 900 mK through a PID control. Note that an aluminum alloy diaphragm with a diameter of 40 mm is placed in front of each band-pass filter of the optical filter set to prevent the blackbody radiation from scattering, and the inner wall of the detector block is coated with Stycast/SiC to further absorb stray light.

3 Results

3.1 Optical and temperature response

The response of a KID to an external field (or multiple fields) such as optical radiation (photons) and thermal phonons is basically the change of the number (or density) of quasiparticles/Cooper pairs in the KID's superconducting inductive line owing to Cooper-pair breaking. The excited quasiparticles will reach a steady-state (with an average number N_{qp}) when the generated ones are equal to the recombined ones, i.e., N_{qp}/τ_{qp} (τ_{qp} is the life time of quasiparticles) [22]. As is well known, the measured KID response is linked with the change of a scattering parameter named S_{21} with respect to microwave readout frequency, corresponding to the change of N_{qp} [8]. Note that S_{21} is usually plotted as an I-Q circle for a better understanding of the KID response, with its radius A (also called resonator amplitude) as a parameter adopted commonly in character-

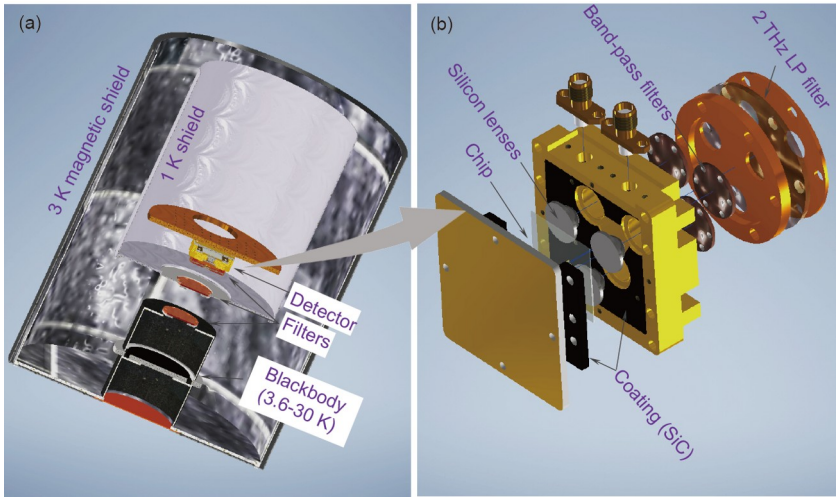

Figure 2 (Color online) (a) Schematic picture of the experimental setup, showing a temperature-variable blackbody, a set of optical filters, and the measured detectors. The temperature-variable blackbody and the optical filter set are placed in front of the detector chip to provide a three-THz-band radiation source. (b) Assembly drawing of the detector module. The silicon lens integrated detector chip is mounted in an oxygen-free copper block thermally anchored to the mixing chamber of a dilution fridge. The inner wall of the block is coated with Stycast/SiC to absorb stray light.

izing the KID response.

Figure 3(a) shows the calculated blackbody radiation at 3.6 and 30 K, i.e., the lowest and highest temperatures of the blackbody, and the measured transmission responses of the optical filter set at the three THz bands by a THz time-domain spectrometer (TDS). Obviously, the dynamic range of the blackbody radiation reaches approximately 10^7 at the 1.4-THz band but reduces considerably at the two lower frequency bands. Combining the blackbody radiation with the transmission response of the THz filter set, we can compute the optical radiation powers incident onto respective elliptical silicon lenses. By varying the blackbody temperature, we measured the transmission response S_{21} of the five KIDs including two dark ones. Note that the mixing chamber temperature is nearly not changed (65 mK) during this measurement. Figure 3(b) and (c) show the measured S_{21} for detector 2 (0.85-THz band) as an example. Obviously, the higher the optical radiation power is, the lower the microwave resonance frequency and the Q factor is owing to increased density of quasiparticles (or decreased density of Cooper pairs) [8]. To verify that the responses of detectors 1, 2, and 3 are attributed purely to the blackbody's optical radiation, we plot the normalized relative resonance-frequency shift ($\delta f/f_0$) against the blackbody temperature for the five KIDs, as shown in Figure 4(a). It can be clearly seen that the normalized relative resonance-frequency shift increases exponentially with the blackbody temperature for detectors 1, 2, and 3, but has an insignificant increase for detectors 4 and 5 (two dark KIDs). The thermal effect caused by optical radiation is therefore negligible. The non-equilibrium optical responsivity $\mathrm{d}A/\mathrm{d}P_{\mathrm{rad}}$ was measured for detectors 1, 2, and 3 by tuning the blackbody temperature in a range of ±100 mK

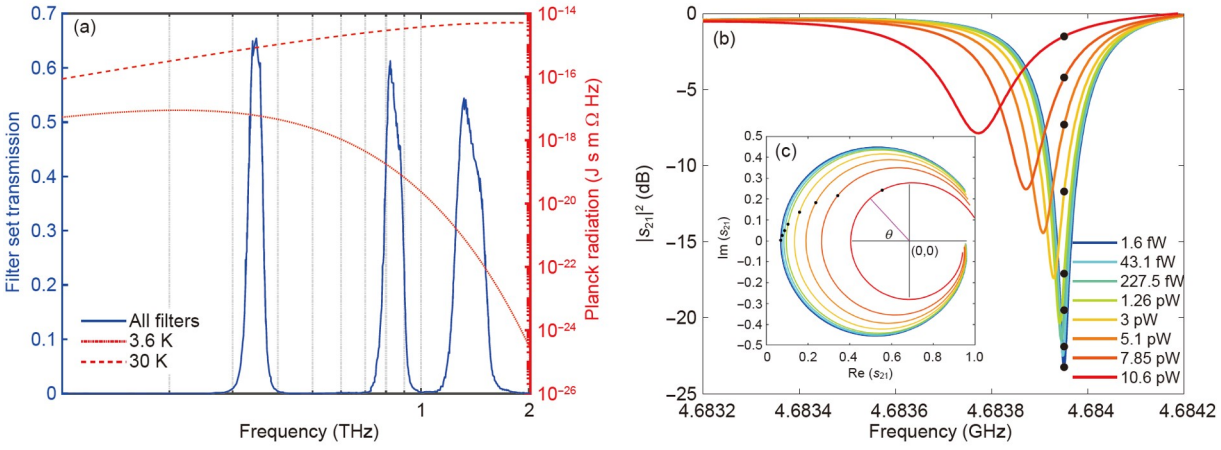

Figure 3 (Color online) (a) Calculated blackbody radiation at 3.6 and 30 K and measured transmission responses of the optical filter set at the three THz bands by a THz TDS. (b) Measured S_{21} for detector 2 (0.85-THz band) at different optical radiation powers. (c) Measured S_{21} for detector 2 (0.85-THz band) plotted as I-Q circles at different optical radiation powers.

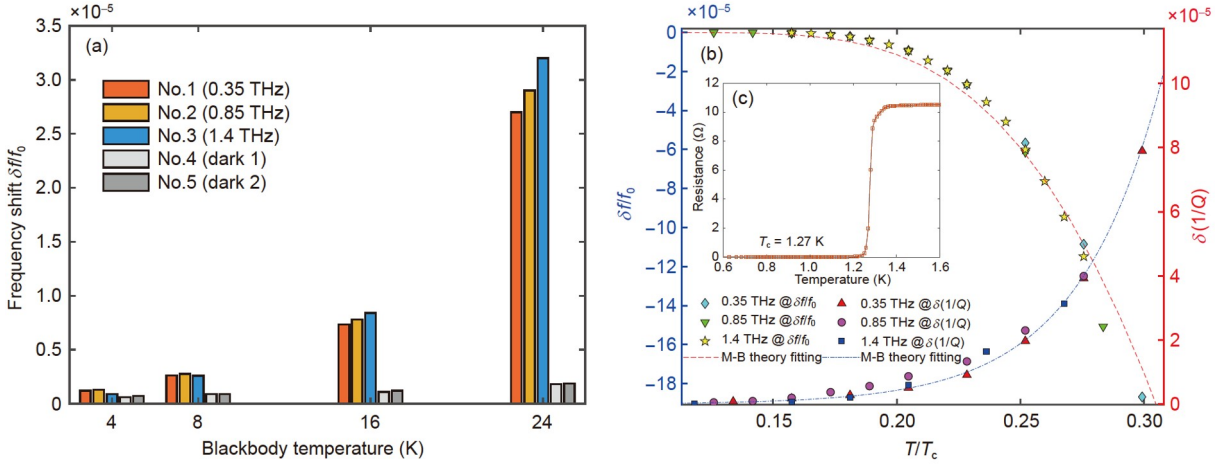

Figure 4 (Color online) (a) Measured relative resonance-frequency shift of the five KIDs at different blackbody temperatures. The resonance-frequency shift increases exponentially for detectors 1, 2, and 3, but has an insignificant increase for detectors 4 and 5. (b) Measured relative resonance-frequency shift and Q-factor change of detectors 1, 2, and 3 as a function of bath temperature. The blue dot line and the red dot line are the calculated results according to Mattis-Bardeen's theory. (c) The measured resistance-temperature curve of the Al film. It has a critical temperature of about 1.27 K.

with a resolution of 1 mK when the bath temperature and microwave readout power are both fixed. We also measured the transmission responses S_{21} of detectors 1, 2, and 3 with respect to the bath temperature (65-350 mK), giving the equilibrium thermal responsivity $\mathrm{d}A/\mathrm{d}T_{\mathrm{bath}}$. The normalized relative resonance-frequency shift and the change of $1/Q$ are plotted in Figure 4(b) together with the fitting results based on the Mattis-Bardeen theory [6]. The fitted kinetic inductance factor is about 2%, which is fairly similar to previous results by our and other groups [23,24].

3.2 Fluctuation of quasiparticles induced by optical radiation

The number of the excited quasiparticles in steady state fluctuates with respect to time, thus resulting in fluctuation in A as well as an orthogonal component (i.e., phase fluctuation) on the plotted I-Q circle. Theoretically, the power spectral density (PSD) of the number of quasiparticles (N_{qp}) obeys the following:

$$S_{\mathrm{A}}(f)=\frac{4N_{\mathrm{qp}}\tau_{\mathrm{qp}}}{1+(2\pi f\tau_{\mathrm{qp}})^2}\left(\frac{\mathrm{d}A}{\mathrm{d}N_{\mathrm{qp}}}\right)^2. \tag{3}$$

This PSD includes both the generated noise and the recombination noise (equal contribution), and holds for quasiparticles from different origins (in equilibrium or non-equilibrium), with $S_{N\mathrm{qp}}(0)$ independent of the bath temperature in equilibrium. As the resonator amplitude A is usually measured, thus its power spectral density $S_A(f)$ is readily available through Fourier transformation for its recorded time series. The relation between the two PSDs is just the square of $\mathrm{d}A/\mathrm{d}N_{\mathrm{qp}}$, which can be computed through $\mathrm{d}A/\mathrm{d}T\cdot(\mathrm{d}T/\mathrm{d}N_{\mathrm{qp}})$ in equilibrium (thermal-phonon induced quasiparticles) and $\mathrm{d}A/\mathrm{d}P_{\mathrm{rad}}\cdot(\mathrm{d}P_{\mathrm{rad}}/\mathrm{d}N_{\mathrm{qp}})$ in non-equilibrium (photon-induced quasiparticles). Note that both $\mathrm{d}A/\mathrm{d}T$ and $\mathrm{d}A/\mathrm{d}P_{\mathrm{rad}}$ are measured, while $\mathrm{d}T/\mathrm{d}N_{\mathrm{qp}}$ and $\mathrm{d}P_{\mathrm{rad}}/\mathrm{d}N_{\mathrm{qp}}$ are usually calculated according to $\mathrm{d}T/\mathrm{d}N_{\mathrm{qp}}=2\Delta^2(\tau_{\mathrm{qp}}/D)^{0.5}/\tau_0N_0\cdot(k_{\mathrm{B}}T_{\mathrm{c}})^3$ and $\mathrm{d}P_{\mathrm{rad}}/\mathrm{d}N_{\mathrm{qp}}=\Delta/(\tau_{\mathrm{qp}}\eta_{\mathrm{opt}}\eta_{\mathrm{pb}})$ [9], respectively.

Figure 5(a) shows the measured $S_A(f)$ for detector 2 (the 0.85-THz band) as an example. Taking the flat noise spectrum roughly between 100 Hz and 1 kHz, which is equal to $4N_{\mathrm{qp}}\tau_{\mathrm{qp}}(\mathrm{d}A/\mathrm{d}N_{\mathrm{qp}})^2$, we can see that it has a positive correlation with the optical radiation power, with the lowest value down to −85 dBc. This positive correlation is understandable as $N_{\mathrm{qp}}\tau_{\mathrm{qp}}\propto V$, with V as an active volume of quasiparticles and being proportional to the diffusion length [25,26], but needs to be further studied since some contradicted results were also reported [17]. From the measured spectra shown in Figure 5(a), we can find that the roll-off frequency (i.e., $1/2\pi\tau_{\mathrm{qp}}$) is also dependent upon the radiation power. By fitting the spectra measured for the three detectors with eq. (3), we obtained their respective lifetime τ_{qp}, as plotted in Figure 5(b). For the 0.85-THz and 1.4-THz KIDs, there are saturated quasiparticle life times of about 100 and 130 μs, respectively, while P_{rad}<1 fW. Their quasiparticle life times are all proportional to $P_{\mathrm{rad}}^{-3.3\pm0.2}$ while P_{rad}>100 fW, This trend is similar to the previous result [9], but with a smaller index. The quality of the fabricated Al superconducting film might account for this difference.

3.3 Noise equivalent power and optical efficiency

The NEP of KIDs can be obtained by measuring S_{A} and $\mathrm{d}A/\mathrm{d}P_{\mathrm{rad}}$ and is expressed as:

$$\mathrm{NEP}(f)=\sqrt{S_{\mathrm{A}}}\left(\frac{\mathrm{d}A}{\mathrm{d}P_{\mathrm{rad}}}\right)^{-1}\sqrt{1+(2\pi f\tau_{\mathrm{qp}})^2}\cdot\sqrt{1+(2\pi f\tau_{\mathrm{res}})^2}, \tag{4}$$

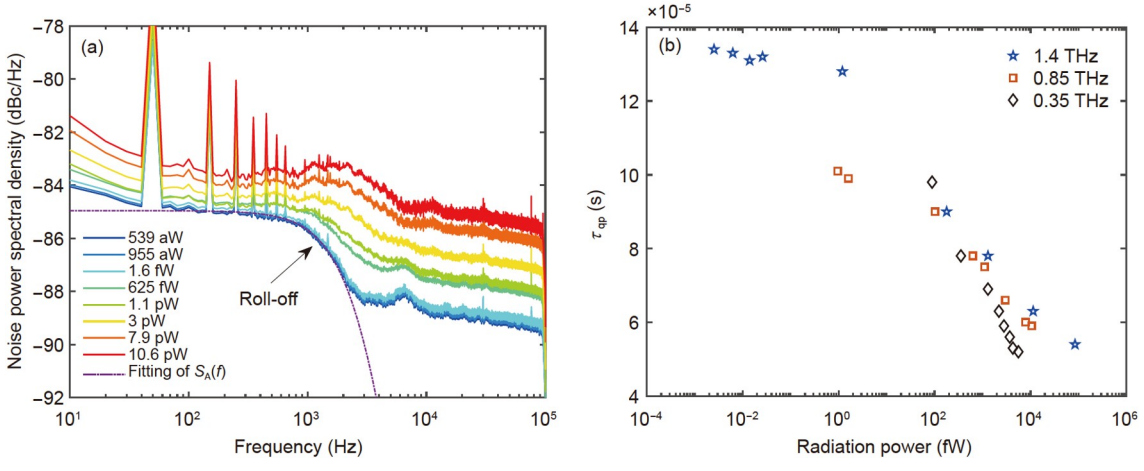

Figure 5 (Color online) (a) Measured $S_{\mathrm{A}}(f)$ for detector 2 (0.85-THz band) at different optical radiation powers, with the case of the lowest radiation power plotted with the corresponding Lorenzen fitting curve as an example. The measurement was performed at a bath temperature of 65 mK and a microwave readout power of −82 dBm. (b) Measured quasiparticle lifetime as a function of radiation power obtained from the roll-off frequencies in the measured spectra.

where τ_{res} (about 1.6 μs in our case) is the resonator's response time and is much shorter than the lifetime of quasiparticles. With the measured S_A, dA/dP_{rad}, and τ_{qp} for detector 1, 2 and 3, we obtain their optical NEPs with respect to P_{rad}. The measured optical NEPs are plotted in Figure 6 together with the photon-noise limited NEP_{photon} and $(NEP_{photon}^2+NEP_{G\text{-}R}^2)^{0.5}$, i.e., the combined photon-noise and G-R noise contribution, which are calculated according to eqs. (1) and (2). Obviously, the three THz KIDs exhibit photon-noise-limited sensitivity at large radiation power (>1 pW) and intrinsic G-R noise at low radiation power (<1 fW). The lowest NEP is approximately 6×10^{-18} W/Hz$^{0.5}$.

Through the fitting of the measured NEPs at large P_{rad} (>1 pW, the linear or photon-noise limited part), we also obtained the optical efficiencies of the three KIDs, equal to 50%, 59%, and 45%, respectively. The antenna-lens models at the three THz bands were simulated by CST Microwave Studio and HFSS, giving their optical efficiencies $\eta_{opt,s}$=49%-56%, which appear in good agreement with the measured ones. Given the fact that the elliptical Si lenses do not have anti-reflection coating (i.e., with a reflection loss of 30%), the actual optical efficiencies can be as high as 70%-80%.

4 Materials and method

4.1 Background noise in Antarctic

For a diffraction limit antenna, $\Omega A = \lambda^2$. Then the noise equivalent power due to the background noise is given by

$$NEP_{BG} = 2\varepsilon k_B T_{BG}\sqrt{\Delta\nu}, \quad (5)$$

where ε is typically equal to 1, k_B the Boltzmann constant, T_{BG} sky radiation temperature (or background temperature), and $\Delta\nu$ the instantaneous detection bandwidth. Taking a relative bandwidth of 10% for the 0.85-THz band ($\Delta\nu$= 85 GHz), a typical winter ground temperature of 220 K at Dome A in Antarctic, and an atmospheric transmission of 0.5 for the 0.85-THz frequency band, we can have T_{BG}=110 K and thus an estimated $NEP_{BG} = 8.8\times10^{-16}$ W/Hz$^{0.5}$.

4.2 Lens antenna efficiency

The center frequency of the twin-slot antennas in detectors 1, 2, and 3 (see Figure 1(a)) is designed at 0.35, 0.85, and 1.4 THz, respectively. Before being coupled with the twin slot antenna, the radiation is focused by an ellipsoid high-resistivity float-zone silicon (FZ-Si) lens, made by Sumipro submicron lathing BV, Netherlands. The ellipsoid silicon lens has a long axis of 4.182 mm and a short axis b of 4 mm. The total optical efficiency of the detector system is given by

$$\eta_{opt,s} = \eta_{cpw}\eta_{match}\eta_{ref}\eta_{SO}, \quad (6)$$

where η_{cpw} is the transmission efficiency of the CPW line, η_{match} the coupling efficiency between the twin-slot antenna and the CPW line, η_{ref} the reflection efficiency of the silicon lens, η_{SO} the efficiency due to the overflow of the integrated lens antenna. The simulated optical efficiencies at the 0.35/0.85/1.4 THz band are 53%, 56% and 49%, respectively.

4.3 Sample preparation

A layer of aluminum with a thickness of 120 nm is evaporated on a 350 μm high-resistivity (ρ>1 kΩ cm) silicon substrate at a rate of 16 Å/s. The Al film has a sheet resistance of 390 mΩ/□, a Residual Resistivity Raito (RRR) of 5.4 and a transition temperature of 1.27 K, corresponding to an energy gap of 193 μeV ($\Delta\approx1.76k_BT_c$). The KID is read out through a coplanar waveguide (CPW) line with a central conductor width of 10 μm and a gap of 6 μm. The normal state resistivity of the CPW line is about 2.9 μΩ cm and the skin depth of the CPW line is 72 nm at 1.4 THz.

4.4 Temperature-variable blackbody and optical radiation

The temperature-variable blackbody is a 70-mm-diameter metal plate coated with carbon-loaded epoxy (EPOTEK 920 1LB part A, containing 3% by weight carbon black and 3% by weight EPOTEK 920 1LB part B) and covered with 0.1

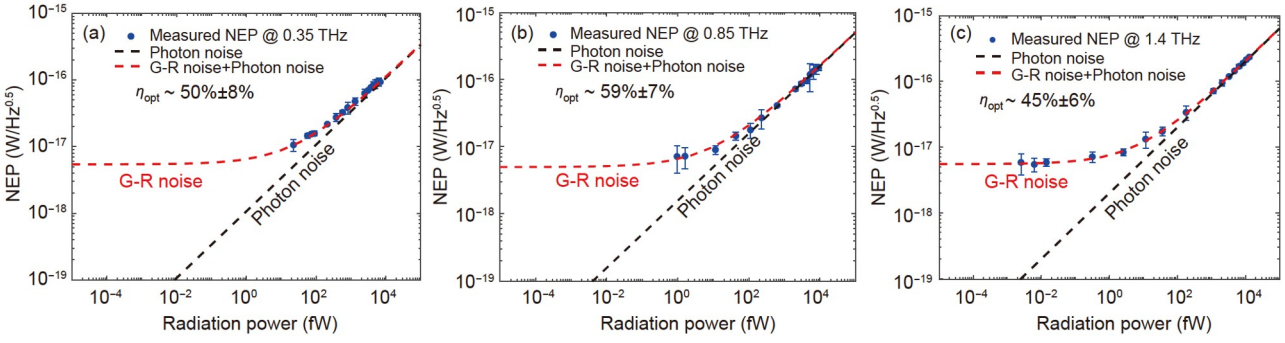

Figure 6 (Color online) Noise equivalent power. Measured optical NEP at (a) 0.35 THz, (b) 0.85 THz, and (c) 1.4 THz for different optical radiation powers. The black dot line is the calculated photon-noise limited NEP photon and the red dot line is the combined photon-noise and G-R noise contribution by eqs. (1) and (2).

and 0.3 mm mixed SiC particles. The temperature-variable blackbody is fixed at the 3 K shield window of the dilution fridge with four 16-mm long and 0.6-mm thick Kevlar wires, giving a thermal conductivity of ~10^{-7} W/K in a wide temperature range of 3.6-30 K. The blackbody is 20 mm from the detector chip and regarded as an extended source. According to Planck's law, the radiation power $P_{\rm rad}$ in front of the detector is

$$P_{\rm rad}(T_{\rm BB}) = \int_0^\infty \frac{{\rm Tr}(\nu) h\nu}{{\rm e}^{\frac{h\nu}{k_{\rm B}T_{\rm BB}}} - 1} {\rm d}\nu, \quad (7)$$

where ν is the photon frequency, ${\rm Tr}(\nu)$ the transmission of the filter as a function of frequency, and $T_{\rm BB}$ the temperature of the blackbody.

4.5 Optical filter set

The optical-filter set is made by QMC Instruments, Cardiff. It consists of three 2-THz low-pass filters (at 3, 1 K and about 100 mK) and three common band-pass filters (at 65 mK) centered at 0.35, 0.85, and 1.4 THz, respectively.

4.6 Responsivity measurement

The responsivity ${\rm d}A/{\rm d}P_{\rm rad}$ of the KID is usually obtained from a linear fit to the response A measured as a function of $P_{\rm rad}$. When the blackbody temperature is swept slowly around the $P_{\rm rad}$, the measurement point will be integrated for 20 ms. The responsivity ${\rm d}A/{\rm d}P_{\rm rad}$ at each blackbody temperature is obtained by fitting the slope of the response in a small dynamic range. Note that the fitting needs to be done in the linear region.

5 Discussion and conclusions

The KID's active volume is required when calculating the two fundamental noise limits given by eqs. (1) and (2). There is a school of thought that the KID's active volume is equal to the cross-section area of the central conductor of the KID's superconducting inductive line multiplied by the half-length of the inductive line [9], i.e., the KID's active length of quasiparticles. This active length in our case was found to be 1220-1830 μm, which is in between the resonator's half-length 3013-3250 μm and the diffusion length 788-898 μm calculated in terms of the measured $\tau_{\rm qp}$. In our case, $\tau_{\rm qp}$ is much shorter than that reported in refs. [9,27-29] for a thin Al superconducting film. As $N_{\rm qp}\tau_{\rm qp} \propto V$, a shorter $\tau_{\rm qp}$ indicates a higher quasiparticle density $n_{\rm qp}$. With a constant active volume, a smaller ratio of $n_{\rm qp}/\tau_{\rm qp}$ is beneficial to the reduction of intrinsic generation-recombination noise. On the other hand, as the photon energy $h\nu$ is much larger than the superconductor's gap energy 2Δ, the recombination term in eq. (1) is in fact negligible. With the reduction of $P_{\rm rad}$ such as broadband imaging spectroscopy and space observations, the photon-noise limit may reach a level even below the G-R noise measured in this work. Further studies on the effect of the Al-film thickness and quality on the detection sensitivity will be done in the future while we still care for the uniformity of large-format arrays.

This work was supported by the National Natural Science Foundation of China (Grant Nos. 11925304, 12020101002, and 11922308), and Chinese Academy of Sciences (CAS) Program (Grant Nos. QYZDJ-SSW-SLH043, GJJSTD20210002, and YJKYYQ20170031).

1 C. K. Walker, *Terahertz Astronomy* (CRC Press, Boca Raton, 2015).
2 K. D. Irwin, and C. H. Gene, *Transition-Edge Sensors* (Springer, Berlin, 2005).
3 P. K. Day, H. G. LeDuc, B. A. Mazin, A. Vayonakis, and J. Zmuidzinas, Nature **425**, 6960 (2003).
4 A. Monfardini, R. Adam, A. Adane, P. Ade, P. André, A. Beelen, B. Belier, A. Benoit, A. Bideaud, N. Billot, O. Bourrion, M. Calvo, A. Catalano, G. Coiffard, B. Comis, A. D'Addabbo, F.-X. Désert, S. Doyle, J. Goupy, C. Kramer, S. Leclercq, J. Macias-Perez, J. Martino, P. Mauskopf, F. Mayet, F. Pajot, E. Pascale, N. Ponthieu, V. Revéret, L. Rodriguez, G. Savini, K. Schuster, A. Sievers, C. Tucker, and R. Zylka, Low Temp. Phys. **176**, 5 (2014).
5 S. C. Shi, S. Paine, Q. J. Yao, Z. H. Lin, X. X. Li, W. Y. Duan, H. Matsuo, Q. Zhang, J. Yang, M. C. B. Ashley, Z. Shang, and Z. W. Hu, Nat. Astron. **1**, 0001 (2016).
6 D. C. Mattis, and J. Bardeen, Phys. Rev. **111**, 2 (1958).
7 M. Dressel, and G. Grüner, *Electrodynamics of Solids: Optical Properties of Electrons in Matter* (Cambridge University Press, Cambridge, 2002).
8 J. Zmuidzinas, Annu. Rev. Condens. Matter Phys. **3**, 169 (2012).
9 P. J. de Visser, J. J. A. Baselmans, J. Bueno, N. Llombart, and T. M. Klapwijk, Nat. Commun. **5**, 3130 (2014).
10 R. W. Boyd, Infrared Phys. **22**, 3 (1982).
11 A. G. Kozorezov, A. F. Volkov, J. K. Wigmore, A. Peacock, A. Poelaert, and R. den Hartog, Phys. Rev. B **61**, 11807 (2000).
12 P. J. de Visser, J. J. A. Baselmans, P. Diener, S. J. C. Yates, A. Endo, and T. M. Klapwijk, Phys. Rev. Lett. **106**, 167004 (2011).
13 C. M. Wilson, L. Frunzio, and D. E. Prober, Phys. Rev. Lett. **87**, 067004 (2001).
14 S. J. C. Yates, J. J. A. Baselmans, A. Endo, R. M. J. Janssen, L. Ferrari, P. Diener, and A. M. Baryshev, Appl. Phys. Lett. **99**, 073505 (2011).
15 R. M. J. Janssen, J. J. A. Baselmans, A. Endo, L. Ferrari, S. J. C. Yates, A. M. Baryshev, and T. M. Klapwijk, Appl. Phys. Lett. **103**, 203503 (2013).
16 L. Ferrari, O. Yurduseven, N. Llombart, S. J. Yates, A. M. Baryshev, J. Bueno, and J. J. A. Baselmans, SPIE Proc. **9914**, 99142G-6 (2016).
17 L. Ferrari, O. Yurduseven, S. J. C. Yates, J. Bueno, V. Murugesan, D. J. Thoen, A. Endo, A. M. Baryshev, and J. J. A. Baselmans, IEEE Trans. Terahertz Sci. Technol. **8**, 99 (2018).
18 J. Hubmayr, J. Beall, D. Becker, H. M. Cho, M. Devlin, B. Dober, C. Groppi, G. C. Hilton, K. D. Irwin, D. Li, P. Mauskopf, D. P. Pappas, J. Van Lanen, M. R. Vissers, Y. Wang, L. F. Wei, and J. Gao, Appl. Phys. Lett. **106**, 073505 (2015).
19 D. Flanigan, H. McCarrick, G. Jones, B. R. Johnson, M. H. Abitbol, P. Ade, D. Araujo, K. Bradford, R. Cantor, G. Che, P. Day, S. Doyle, C. B. Kjellstrand, H. Leduc, M. Limon, V. Luu, P. Mauskopf, A. Miller, T. Mroczkowski, C. Tucker, and J. Zmuidzinas, Appl. Phys. Lett. **108**, 083504 (2016).
20 J. Gao, J. Zmuidzinas, A. Vayonakis, P. Day, B. Mazin, and H. Leduc, J. Low Temp. Phys. **151**, 1 (2008).

21 S. Friedrich, K. Segall, M. C. Gaidis, C. M. Wilson, and D. E. Prober, Appl. Phys. Lett. **71**, 26 (1997).
22 S. B. Kaplan, C. C. Chi, D. N. Langenberg, J. J. Chang, S. Jafarey, and D. J. Scalapino, Phys. Rev. B **14**, 4854 (1976).
23 T. G. Phillips, and J. Keene, IEEE Proc. **80**, 11 (1992).
24 J. Zmuidzinas, and P. L. Richards, IEEE Proc. **92**, 10 (2004).
25 H. Kraus, F. von Feilitzsch, J. Jochum, R. L. Mossbauer, T. Peterreins, and F. Probst, Phys. Lett. B **231**, 1 (1989).
26 J. Jochum, H. Kraus, M. Gutsche, B. Kemmather, F. V. Feilitzsch, and R. L. Mössbauer, Ann. Phys. **505**, 7 (1993).
27 J. Baselmans, S. J. C. Yates, R. Barends, Y. J. Y. Lankwarden, J. R. Gao, H. Hoevers, and T. M. Klapwijk, Low Temp. Phys. **151**, 1 (2008).
28 R. Barends, J. J. A. Baselmans, S. J. C. Yates, J. R. Gao, J. N. Hovenier, and T. M. Klapwijk, Phys. Rev. Lett. **100**, 257002 (2008).
29 J. J. A. Baselmans, and S. J. C. Yates, AIP Conf. Proc. **1185**, 1 (2009).